Enhanced Fog Water Harvesting on Superhydrophobic Steel Meshes

Pegah Sartipizadeh, Mohammad Reza Mohammadizadeh,* Carlo Antonini, and Raziyeh Akbari*

Fog water harvesting, inspired by desert organisms, offers a sustainable and low-cost solution to water scarcity, especially in humid coasts. Mesh-based fog collection is gaining research attention due to its passive operation and minimal environmental impact. This study aims to develop effective, low-cost, scalable, and easy-to-apply fog harvester designs while evaluating their performance under fog conditions that closely mimic real-world scenarios. Copper is electrodeposited onto steel meshes to create a rough hydrophobic layer, and modified with a per- and polyfluoroalkyl substances-free silica-sol to reach superhydrophobicity. The modified sample achieves a water harvesting efficiency of 580 mg $(cm^2h)^{-1}$, a 40% improvement over uncoated steel meshes, comparable to the results of single-drop impact studies and fog water harvesting investigations. The key considerations for fog harvesting research, emphasizing the need to calculate fog harvesting efficiency as the ratio of collected water to available atmospheric water generated in experimental setups are highlighted. Without standardized testing protocols, inconsistent results hinder progress and divert focus from real-world applications. To address this, a methodology for a standardized protocol reflecting fog characteristics and environmental conditions is developed. This technological advancement offers a viable strategy to mitigate water scarcity through optimized fog water harvesters based on surface property design and control.

P. Sartipizadeh, M. R. Mohammadizadeh
Supermaterials Research Laboratory (SRL)
Department of Physics
University of Tehran
North Kargar Ave., P. O. Box 14395-547 Tehran, Iran
E-mail: zadeh@ut.ac.ir

C. Antonini, R. Akbari
Surface Engineering and Fluid Interfaces Laboratory (SEFI Lab)
Department of Materials Science
University of Milano-Bicocca
20126 Milan, Italy
E-mail: raziyeh.akbari@unimib.it

The ORCID identification number(s) for the author(s) of this article can be found under https://doi.org/10.1002/adem.202402378.

1. Introduction

The global clean water shortage crisis stands as one of the most urgent challenges of our time, intensifying other major issues such as climate change and air pollution.[1] This crisis is particularly critical in arid regions, including countries like Italy, Iran, and those in the Persian Gulf, where water scarcity poses severe threats to both human populations and the environment. One promising source of clean water is fog, which is used for a few million years by desert animals and plants.[2–6] In the Atacama Desert of Chile, where rainfall can be absent for years, the clouds contain an average of 13.8 kg m^{-2}.[7] By harnessing just a few percent of this resource, the region could potentially satisfy the country's entire annual water consumption needs.[7–9] These meshes offer a passive method of water collection, though their efficiency decreases in low humidity conditions.[10] Despite this limitation, researchers and engineers worldwide are working to enhance this technology because of its straightforward design, low cost, reliance on renewable energy, and minimal environmental impact, with no associated noise, heat, or air pollution.[11,12] These advantages have made water harvesting a compelling area of research, as evidenced by the substantial growth in academic publications on water harvesting and fog collection in recent years, as visually represented in **Figure 1** for details.

Atmospheric water harvesting can be achieved from two primary sources: vapor and fog. Harvesting water from vapor (uncondensed water) typically involves a phase change process, where water is condensed by creating a temperature difference or captured chemically using hygroscopic materials.[11] Collecting vapor by dew harvesting, which is particularly effective in areas with relative humidity lower than 100% and environmental temperature, relies on materials like graphene oxide or specific polymers that absorb moisture and condense water vapor.[13–16] Additionally, passing humid air through cold refrigeration coils cools the air, causing water vapor to condense.[17] In contrast, fog liquid droplets have a diameter typically less than 40 μm and fog water harvesting can be achieved by capturing directly the liquid, without condensation, thus requiring no energy input.[11,18] Fog water harvesting meshes are especially effective in regions with high relative humidity (typically above 75%) condition, ideal for coastal deserts.[19]

**ADVANCED
SCIENCE NEWS**

www.advancedsciencenews.com

**ADVANCED
ENGINEERING
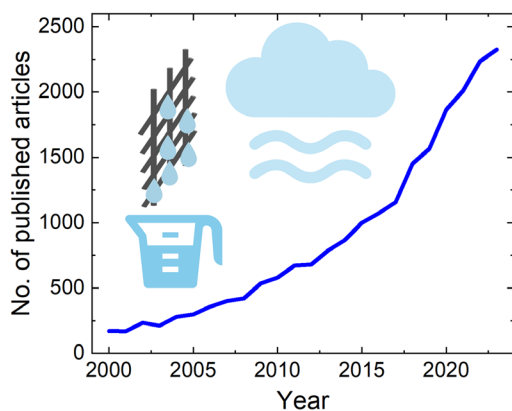MATERIALS**

www.aem-journal.com

Figure 1. Statistics related to water harvesting and fog collection, extracted from Scopus, show an increase in articles published from 2000 to 2023. The following keywords were used to extract results: for "Water harvesting"- {water} AND {harvesting}; for "Fog collection"- {fog} AND {collection}. A schematic of fog water harvesting by meshes inserted in the figure.

Extracting water from fog using a collector involves three main steps: 1) capture of tiny fog particles within the collector; 2) transport of particles, which can first merge to form larger droplets without exceeding the optimal size related to the mesh pore size; and 3) drainage to the reservoir.[13,20,21] If any of these steps are not executed effectively, the overall efficiency of the process declines: as such, all steps need optimization. Fog harvesters are more feasible when designed as meshes due to their open-porous structure, which reduces the surface area obstructing airflow. This design results in lower drag and a smaller aerodynamic coefficient compared to solid sheets. Additionally, mesh porosity, wire diameter, and airflow conditions significantly influence performance. Combined open-porous structure with woven wires in meshes effectively captures fog particles, ensuring an efficient initial step in fog collection. Meshes also facilitate directional transport of collected droplets, a feature less efficient in solid collector sheets. However, a key challenge with mesh designs is pore clogging, which can hinder long-term performance and reduce overall harvesting efficiency.[22,23] This occurs due to the capillary effect in the pores, causing the pores to remain filled even after the drainage step. As a result, subsequent fog particles cannot be effectively captured by the mesh because the pores become clogged, leading to a reduction in the mesh's aerodynamic efficiency and, consequently, its water collection capacity. Hydrophobizing meshes are an effective technique to mitigate clogging; however, superhydrophobicity can lead to droplet re-entrance. This occurs because the low adhesion force of the droplets causes them to roll off the mesh wire surface.[9]

The parameters that influence the harvesting efficiency of fog collectors can be categorized into three main groups: 1) fog characteristics (e.g., concentration, temperature, and flow rate), 2) prevailing wind characteristics (e.g., speed, direction, and gradient), and 3) mesh geometry and surface characteristics (e.g., knot shape, pore size, wire thickness, material, and surface morphology and wettability).[4,11,13,22] The diameter of fog particles in nature varies from 5 to 50 μm, depending on factors such as the temperature difference between the environment and the

dew point, and the type of fog (e.g., advection fog, radiation fog, and evaporative fog).[11] For instance, lowering the air temperature below the dew point increases dew and fog formation by condensing water vapor. Fog harvester efficiency also depends on the size of the fog droplets. Schemenauer et al. discovered that the efficiency for larger particles (15 μm) increased more rapidly with rising wind speed compared to smaller particles (11 μm).[24] In this regard, there is an optimal window of relatively low wind speed ($<2\,\mathrm{m\,s^{-1}}$) to collect more water by meshes, with lower wind speeds being more effective for meshes with smaller pore sizes.[25,26] Indeed, the average prevailing wind speed in the fog season of the coasts around the world is in a similar range.[27]

Surface geometry and dimensional characteristics highly affect the water drop dynamics on the surface, and eventually, the amount of water collected from fog.[28–30] Some studies including Wang et al.[31] and Yin et al.[32] found that in a similar mesh number, thinner wires led to higher fog water harvesting efficiency and faster collection due to the reduced capillary. Pores clog easier when the fog droplet size is comparable to the pore size, due to an increase in the pore capillary effect, interrupting the transportation step and expediting the drainage, reducing the fog water harvesting efficiency. In addition, a successful fog water harvesting system relies on appropriate micro–nano structures on the mesh wires with optimal surface properties.[4,28,33] On rough superhydrophobic surfaces with contact angle larger than 135° and a hysteresis angle smaller than 20°, water droplets form on prominences while air bubbles get trapped in indentations, leading to a Cassie–Baxter state. The trapped air prevents water from penetrating nanostructures, increasing contact angle, boosting the transportation and drainage steps, thus enhancing fog water harvesting efficiency, the larger the fog droplet size, the more hydrophobicity is required.[34–37]

In this study, copper layers were electrodeposited onto stainless steel meshes and further chemically modified with hydrophobic silanes. Samples with varying mesh dimensions, micro–nano surface structures, and wettability modifications, i.e., hydrophobic and superhydrophobic coatings, were examined through characterization experiments and a homemade fog water harvesting test setup. These experiments elucidated optimal mesh characteristics and test conditions for enhancing fog collection. Finally, a thorough comparison with existing literature with similar sample properties and test chamber designs was conducted to outline expectations and future perspectives for fog collection using hydrophobic and superhydrophobic meshes.

2. Experimental Section

2.1. Sample Preparation

To assess the size effect on fog collection, water harvesting tests were conducted on five square woven meshes with pore sizes of 50, 100, 250, 425, and 600 μm, and wire thickness of 50, 60, 130, 150, and 180 μm, respectively; the corresponding shade coefficients, defined as portion of the mesh area covered by wires, were 75, 61, 57, 46, and 42%, respectively. Stainless steel meshes (SS 304) were cut into $3 \times 3\,\mathrm{cm^2}$ pieces and sequentially rinsed in soap, water, acetone, and ethanol, each for 15 min with stirring. The substrates were then immersed in a 10 wt% H_2SO_4 solution

for 30 s to remove surface oxides. To fabricate rough micro–nano structures, a copper layer was electrodeposited onto the substrates, similar to our previous studies.[38] The electrolyte solution contained 0.2 M CuSO₄·5H₂O (99%, Samchun Chemicals) and 0.25 M H₂SO₄ (98%, Parsian Pure Chemical). A two-electrode cell was utilized for electrodeposition, with the steel mesh as the cathode (substrate) and a copper sheet as the anode. The electrolyte temperature was maintained at $45 \pm 5\,°C$ during deposition using a heat bath. Electric current was applied to the electrodes using a Keithley model 6221 current source. Through our previous studies on the electrodeposition of copper, we found that various rough surfaces with dendrite or hierarchical structures with hydrophobic properties can be created by using DC, cyclic voltammetry, or pulse methods.[39] Accordingly, in the present study, electrodeposition methods with various waveforms have been utilized to fabricate rough Cu coatings on the steel meshes. In this regard, waveforms with shapes including square, ramp, sinusoidal, and DC with varying current density and duty cycles have been used, the deposition conditions of the successful samples are summarized in **Table 1**.

Similar to the reaction conducted in ref. [40], the silica solution for modifying the samples was prepared by adding 2.1 mL of Tetraethoxysilane (TEOS, >98%, Exir Company) to 30 mL of ethanol (99.5%, Scharlau) and stirring vigorously for 10 min. Then, 2 mL of Hexamethyldisilazane (HMDS, >99%, Sigma-Aldrich) was slowly added to the solution and the mixture was stirred for 30 min. 3 mL of deionized water was added dropwise to the solution at the same stirring rate at room temperature (≈25 °C). The reaction mixture was stirred constantly for 2 h to form a transparent sol. After immersing the substrates in the sol for 15 min, the samples were rinsed with ethanol.

2.2. Characterization

The static and quasi-static, i.e., advancing and receding, contact angles, contact angle hysteresis, and sliding angles were measured on all samples using a homemade setup equipped with a Veho VMS-004 Deluxe camera, and repeated at least 5 times. The static contact angle was measured using 6 µL deionized water droplets placed on the sample. To measure quasi-static contact angles, a 3 µL water droplet was placed on the sample. The droplet volume was slowly increased ($\approx 10\,µL\,min^{-1}$) to

15 µL to measure advancing contact angles. Then, liquid was withdrawn at the same rate ($\approx 10\,µL\,min^{-1}$), and receding contact angles were measured as the droplet contact area began to shrink. Additionally, the study examines the sustained wetting of both dry and prewetted meshes by assessing the duration that a water droplet maintains its original shape on the surface. The microstructure of the prepared samples was examined using a field-emission scanning electron microscope (FESEM, TESCAN MIRA 3 LMU). Energy dispersive spectroscopy (EDS) was used to analyze the chemical elements of the samples. Additionally, the crystalline phase of the deposited layer was determined by X-ray diffraction (XRD, STOE, Stadi/p, Germany).

2.3. Fog Water Harvesting Test Setup

To evaluate the fog water harvesting performance of the prepared samples, a home-made fog water harvesting test setup had been employed. The setup installed of a large glass chamber measuring $60 \times 100 \times 150\,cm^3$, connected to a ventilator to prevent humidity saturation in the chamber in the vicinity of the sample. As sketched in **Figure 2**a, fog was produced using a humidifier (Emsig, model US 408 plus) at a rate of 210 mL h⁻¹ with a nominal fog droplet size distribution of 1–5 µm. The water flow rate (calculated as the average over a two-hour test) remained constant across all fog collection tests, independent of the air speed in the wind tunnel. A cylindrical wind tunnel, consisting of two concentric steel mesh cylinders 50 cm in length and 8 cm in diameter, was used to simulate wind on a laboratory scale, directing the fog output from the humidifier. The samples were placed on one side of the tunnel, while a variable-speed fan on the other side pushed the fog toward the samples. The samples were secured in holders positioned above water collection containers (Figure 2a,b).
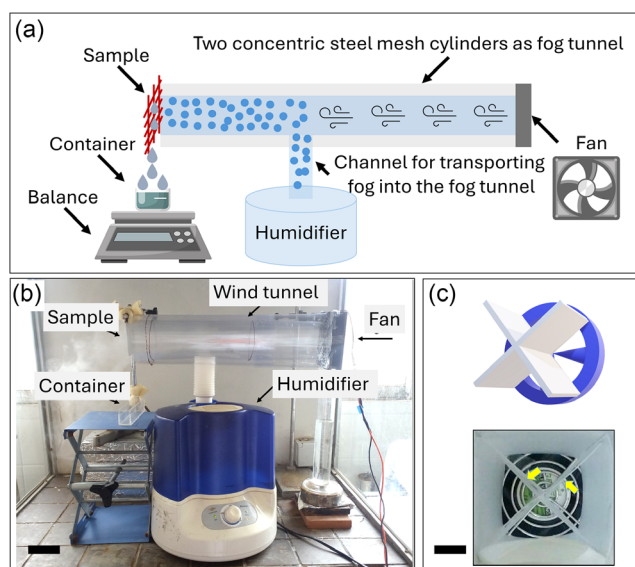
Table 1. Details of the deposition conditions of the sample sets.

Set	Waveform	Current density [mA cm⁻²]	Duty cycle [%]	Deposition time [min]
#1	Square	11.6	90	120
#2	Square	11.6	90	60
#3	Square	11.6	50	60
#4	Ramp	11.6	50	60
#5	Sinusoidal	11.6	100	60
#6	DC	44.4	100	15
#7	DC	11.6,77.7	100	60,5

Figure 2. a) Schematic diagram of the fog water harvesting setup, b) a picture taken from the experimental setup, and c) interior view of the wind tunnel with diagonal plates to reduce vorticity in airflow. Black bars in (b) and (c) show 5 and 2 cm, respectively. The wind tunnel has an outer diameter of 8 cm and a length of 50 cm.

This arrangement was inspired by other research studies.[33,34] The fog flows through a 15 cm-long channel to reach the sample. During preliminary tests, flow swirl caused the fog to not reach the surface of the samples uniformly. To address this issue, two plastic plates were installed in a crosswise configuration in front of the fan to eliminate wind vorticity (Figure 2c).

During the fog water harvesting experiments, the ambient temperature was ≈33 ± 3 °C, with a relative humidity of 26 ± 5% in the chamber and 80 ± 5% at the front of the fog tunnel. Each test lasted 2 h, after which the amount of collected water was weighed. Due to the large scale of the experiment and the resulting high error percentage, each test was repeated at least five times. The average water collection value and error bars were then recorded for each sample. During each experiment, ≈400 g of water was generated by the humidifier. However, the amount of water collected was ≈10% of the generated water, depending on the sample. Fog water harvesting efficiency (η) is calculated as follows in (mg cm^{-2}h^{-1}):[41]

$$\eta = \frac{\text{Total amount of collected water}}{\text{Mesh surface area} \ \times \ \text{Test duration}} \quad (1)$$

In addition, to gain a deeper understanding of the fog collection process and investigate how different surface modifications impact harvesting efficiency, the weight and falling frequency of the drained droplets from the mesh were analyzed, inspired by ref. [42]. To conduct this study, two key parameters were defined and measured: 1) The weight of the droplets that drained from the mesh over a short period, referred to as the "mass of dripping droplets", 2) the time interval between successive droplet drainage events from the sample, referred to as the "cycle of droplets dripping". These parameters were measured during three different stages of a 2 h fog water harvesting experiment: 1) the initial minutes, 2) after 1 h, and 3) the final minutes of the test. A video recording was used to calculate the average time interval between at least five droplet drippings. Additionally, the droplets were collected on a glass slide and weighed to determine their average weight.

3. Results and Discussion

3.1. Effect of Mesh Geometry and Wind Speed

Figure 3a illustrates the fog water harvesting efficiency of meshes with pore sizes of 50, 100, 250, 425, and 600 μm, combined with various wire diameters. These configurations result in shade coefficients ranging from 75% for the mesh with the smallest pore size and thinnest wire to 46% and 42% for meshes with 425 and 600 μm pore sizes, respectively. According to Figure 3a, at a constant wind speed of 0.3 m s^{-1}, the meshes with 425 and 600 μm pore sizes demonstrated significantly higher fog water harvesting efficiency compared to those with smaller pore sizes. This result aligns with previous studies, which suggest that optimal fog collection efficiency is achieved when the shade coefficient is ≈50%.[4,18,28] However, this optimal value also depends on factors such as mesh wettability and fog flow characteristics, including droplet size distribution, fog flow rate, and wind speed. To investigate the effect of droplet size on fog collection efficiency, a second humidifier (Vurf, SPS-808) was employed. This humidifier generated a broader droplet size distribution with a larger nominal droplet size of 10–15 μm. The fog flow produced by this new humidifier exhibited more unsteady behavior. As shown in Figure S1, Supporting Information, under similar fog flow rates and wind speeds, increasing the average droplet size slightly improved the fog collection efficiency of the 600 μm mesh compared to the 425 μm mesh. This contrasts with results for smaller droplet sizes. However, these measurements are less accurate than those obtained for smaller droplets. In the following, the influence of wind speed on the fog water harvesting efficiency on these meshes had been investigated by changing the power applied to the fan to generate four different wind speeds of 0.1, 0.2, 0.3, and 0.4 m s^{-1}. These wind speed numbers were measured by recording a video of the fog entering and exiting the tunnel, then calculating the ratio between the distance traveled by the fog and the recorded time. Figure 3b indicates that the highest fog water harvesting efficiency was achieved at a wind speed of 0.3 m s^{-1} in the mesh with 425 μm pore size, which is lower than the optimal wind speed proposed by Fernandez et al.[25] Considering that their study found smaller pore sizes lead to higher fog water harvesting efficiency at lower
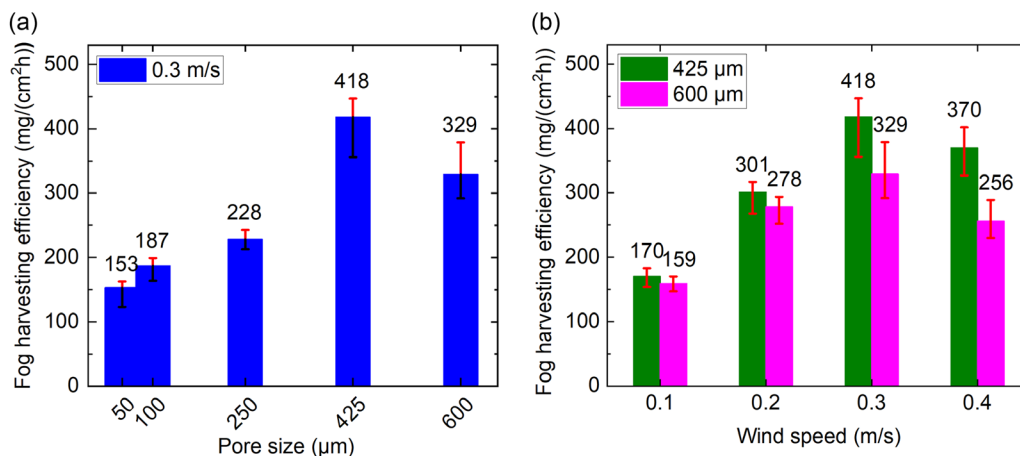

Figure 3. Fog water harvesting efficiency η of meshes a) with different pore sizes and b) in different wind speeds.

wind speeds, and the smallest pore size in their study was 0.051" (1300 µm), it is reasonable to expect that the optimal wind speed for the 425 µm meshes in this study would be significantly lower than what was suggested by Fernandez et al. although fog droplet size must also be taken into consideration.[25] As a result of these experiments, a wind speed of 0.3 m s^{-1} and a mesh pore size of 425 µm were selected as the optimal operating parameters for the subsequent experiments.

3.2. Effect of Electrodeposition Condition and Silica-Sol Modification

As described in Table 1, after selecting the mesh with 425 µm pore size as the suitable substrate, seven sets of samples were fabricated using different electrodeposition conditions and modified with silica solution. Scanning electron microscopy (SEM) images from the surface structure of the mesh wires in the samples also provided in Figure S2, Supporting Information. According to Table 1, a square waveform was used to fabricate the first three sets of samples. In set #2, the deposition time was reduced, and in set #3, the duty cycle was decreased, compared to set #1. All these three sets of samples exhibit nonuniform grain sizes on the surfaces, ranging 1–8 µm in length, as revealed by the SEM images in Figure S2, Supporting Information. Ramp and sinusoidal waveforms were used to fabricate sets #4 and #5, respectively. These resulted in long cracks on the wires compared to the other samples, as shown by the SEM images in Figure S2, Supporting Information. To achieve a more intense deposition with a rougher surface and more uniform grain sizes, DC electrodeposition with higher current densities was employed in sets #6 and #7. In set #6, a current density of 44.4 mA cm^{-2} was applied to the system for 15 min, resulting in pyramids with sharp tips, smaller grains, and a more uniform grain size distribution. Set #7 involved a two-step process: first, a low current density with a long deposition time to evenly cover the wire surface, followed by a quick electrodeposition at seven times higher current density to inhibit further lateral growth and promote columnar growth, generating prominent hemisphere-shaped grains.

The wetting and fog water harvesting efficiency of these seven sets of samples, along with their silica-sol modified counterparts, were characterized to identify the best sample set with optimal wetting state and fog water harvesting performance in both the Cu-coated and Si-Cu-coated conditions. **Figure 4** represents the advancing and receding contact angles, sliding angle, and fog water harvesting efficiency of these samples over five test repetitions. Among the Cu-coated meshes, see Figure 4a, only set #6 exhibited water droplet shedding from the surface, while the water droplet remained sticky on the other six samples. Set #6 also showed the largest advancing and receding contact angles, resulting in lower wetting hysteresis, and higher hydrophobicity. The hydrophobicity in Cu-coated samples can be attributed to the hydrocarbon adsorption on the surface during one week of drying in ambient condition, as observed previously in metal-based coatings.[43–46] This effect is more pronounced when the surface contains grains with elongated vertical structures and sharper tips, such as the pyramids observed in set #6. In terms of fog water harvesting efficiency, see Figure 4c, the Cu-coated samples exhibited efficiencies ranging from 210 to 344 mg cm^{-2}h^{-1}, lower than uncoated steel mesh with 425 µm pore size, shown in Figure 3b, with no direct correlation between hydrophobicity and fog water harvesting efficiency. However, samples #3 to #6, with lower wetting hysteresis (≈50°) compared to the other samples, demonstrated higher efficiency values on average.

According to Figure 4b, after surface modification with silica-sol, all samples became superhydrophobic, with advancing contact angles greater than 140° and sliding angles below 20°, resulting in a significant increase in fog water harvesting efficiency compared to Cu-coated samples, see Figure 4c. Sample #6 stood out as the most hydrophobic, with the highest advancing and receding contact angles, the lowest wetting hysteresis, and the lowest sliding angle among all samples. This sample also achieved the highest average fog water harvesting efficiency of 580 mg cm^{-2}h^{-1}. Notably, to investigate the effect of microstructure on fog collection, silica-sol was directly applied to steel mesh. While its wetting characteristics were similar to those of the Si-/Cu-coated samples, it exhibited a lower water collection rate, with a more pronounced error (e.g., 505 ± 54 mg (cm^{2}h)$^{-1}$), highlighting the importance of surface roughening for optimal performance. Therefore, the samples in set #6 were selected for further study on surface morphology, wetting characteristics, and fog water harvesting performance in the following sections, due to their uniform pyramid shape surface grains, higher hydrophobicity, and higher fog water harvesting efficiency, compared to the rest of the sample sets.
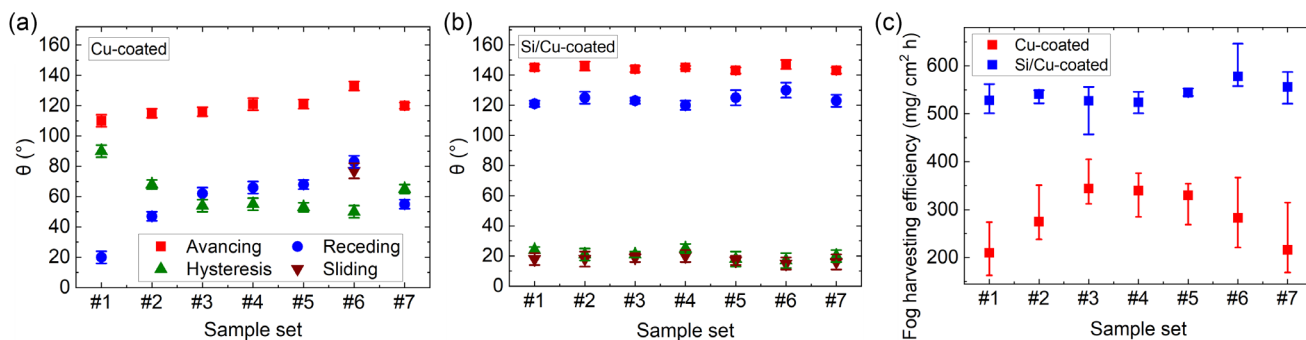

Figure 4. Wetting characteristics of the a) Cu-coated and b) Si-/Cu-coated samples from seven sample sets, along with c) the fog harvesting efficiencies of those sample sets.

3.3. Effect of Surface Modification

To investigate the effect of surface morphology and chemical composition on the fog water harvesting efficiency of coated steel meshes, three different samples were examined: 1) steel mesh, 2) Cu-coated mesh from set #6, and 3) Si-/Cu-coated mesh from set #6. EDS analysis revealed that the Cu-coated mesh was 97% covered with copper, with only 3% oxidation, see Table S1, Supporting Information. The Si-/Cu-coated mesh exhibited a negligible amount of silicon. XRD analysis of the Cu-coated mesh confirmed the polycrystalline nature of the coating, consisting predominantly of pure copper and copper oxide. Additional details can be found in Figure S3, Supporting Information.

SEM images of the samples are presented in **Figure 5**a1–c1. The steel mesh wires exhibited a nearly smooth surface, while the electrodeposition of copper resulted in a dense aggregation of micrometric copper grains with pyramid-like shapes and sharp tips, ranging in size from 2 to 4 µm. The subsequent coating with the pH = 8 silica solution likely contributed to copper layer corrosion, leading to the formation of deep sub-micrometer holes, increasing porosity, enhancing air trapping within the structure.

Water contact angle measurements, presented in Figure 5a2–c2, reveal that while water droplets penetrate and become trapped in the steel mesh, the copper electrodeposition significantly reduces liquid penetration into the mesh pores. This treatment increases the advancing and receding contact angles to 133° and 83°, respectively, resulting in a wetting hysteresis of 50°, and a sliding angle of 77°. The combination of high wetting hysteresis and the need for a high tilting angle for liquid drop shedding is characteristic of a parahydrophobic surface, which exhibits both a high contact angle and strong adhesion, indicating a Wenzel wetting state.[47] Further surface modification with a silica sol resulted in the fabrication of a superhydrophobic mesh, with advancing and receding contact angles of 147° and 130°, respectively, and a reduced hysteresis of 17°. Water droplets easily shed from this sample at a sliding angle of less than 15°. The presence of a thin hydrophobic silica layer on the Si-/Cu-coated mesh, combined with deep sub-micrometric holes within the structure, creates a slippery surface with low surfa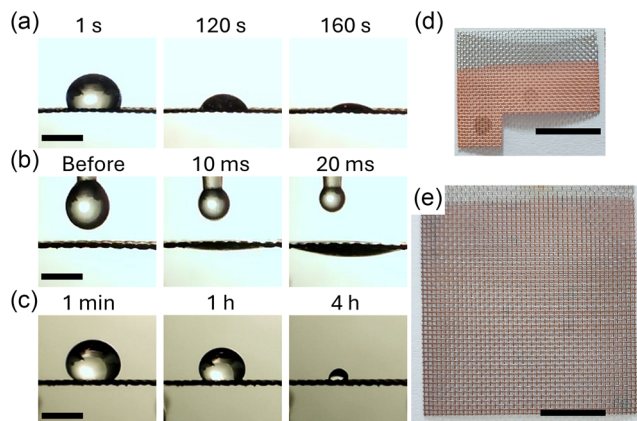ce energy. This configuration traps a higher amount of air within the structure, reducing the tendency of water droplets to adhere.[47]

Figure 6 shows the sustained wetting of both dry and prewetted meshes by evaluating how long a water droplet retains its initial shape on the surface. After placing the droplet on the mesh, its shape is influenced by factors such as penetration, absorption, or evaporation. As depicted in Figure 6a, the contact angle of the water droplet on the dry Cu-coated mesh decreases significantly after 160 s. The droplet leaves behind a darker spot on the Cu-coated sample after being absorbed into the mesh, as shown in Figure 6d. Copper, like many metals, is naturally hydrophilic, with a very high surface energy (≈ 1490 mJ m^{-2}).[48] When copper is electrodeposited from an aqueous solution, the fresh sample initially exhibits hydrophilic properties. However, after drying in the environment, the wetting state of the sample can change depending on surface structure and roughness, as previously observed.[39,49] On a rough Cu-coated sample, the water contact
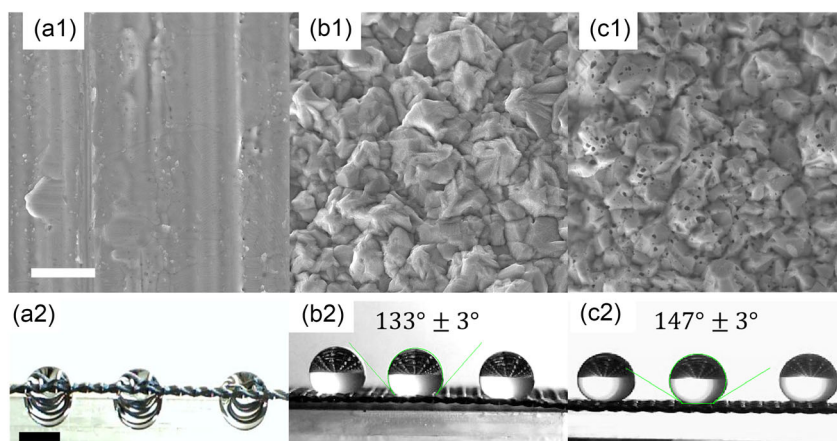

Figure 6. Sustained wetting of samples: a) Cu-coated mesh in a dry state; b) Cu-coated mesh in a wet state; c) Si-/Cu-coated mesh in a dry state. The moments after depositing the droplet at which the pictures were taken are indicated above each. Images of the meshes in (a,c) after the sustained wetting test are shown in d,e), respectively. The black scale bar corresponds to 2 mm in (a–c), and 1 cm in (d,e).

Figure 5. SEM images of the surface and pictures from water droplet on the a1,a2) steel, b1,b2) Cu-coated, and c1,c2) Si-/Cu-coated meshes, respectively. The static contact angle on the samples is written on (a1–c1). Scale bars in (a1,a2) correspond to 5 µm and 2 mm, respectively.

**ADVANCED
SCIENCE NEWS**

www.advancedsciencenews.com

**ADVANCED
ENGINEERING
MATERIALS**

www.aem-journal.com

angle can increase to hydrophobic or even superhydrophobic levels over a few weeks postdeposition. It is hypothesized that this superhydrophobicity on metal surfaces arises from the absorption of hydrocarbons present in the environment.[43–46] During wetting experiments, when the surface comes into contact with water, the liquid removes the thin hydrocarbon layer, exposing the underlying copper. This interaction leads to the formation of copper oxide (CuO_x), which appears as a darker shade of red compared to pure copper.[49] The prewetted Cu-coated mesh quickly absorbs water, see Figure 6b.

As shown in Figure 6c, the sustained wetting test on the Si-/Cu-coated mesh demonstrates that the silica layer effectively acts as a robust barrier against water. As a result, a water droplet on the dry Si-/Cu-coated mesh resists absorption for over 4 h. After this extended period, the water droplet did not penetrate or get absorbed by the mesh but instead dried. The image of the Si-/Cu-coated mesh after the sustained wetting experiment, shown in Figure 6e, reveals no visible trace of the water droplet, in contrast to the Cu-coated mesh. Additionally, due to the superhydrophobic nature of the Si-/Cu-coated mesh, it was not possible to take the sustained wetting test in the prewetted condition.

The fog water harvesting performance of the samples is presented in **Figure 7**. The left vertical axis in this figure displays the mass of dripping droplets versus the cycle of droplets dripping, providing a comparative illustration alongside fog water harvesting efficiency as the right vertical axis in the same plot. The specific values and error bars are detailed in Table S2, Supporting Information. According to Table S2, Supporting Information, the first droplet drips from the steel mesh after 185 s, from the Cu-coated mesh after 280 s, and from the Si-/Cu-coated mesh after 150 s. The mass of droplets decreases over time for both the steel mesh and Cu-coated mesh, with the Cu-coated mesh showing a greater reduction in droplet mass (20%) compared to the steel mesh. This reduction is attributed to the significant filling of the Cu-coated mesh pores during the test. As these pores become filled with water, the mesh collects fog particles less effectively, leading to a decrease in fog water harvesting efficiency. In contrast, the droplets from the Si-/Cu-coated mesh maintain a consistent mass throughout the experiment, indicating the high wetting sustainability and fog water harvesting performance of the sample. While the dripping droplets from the steel mesh
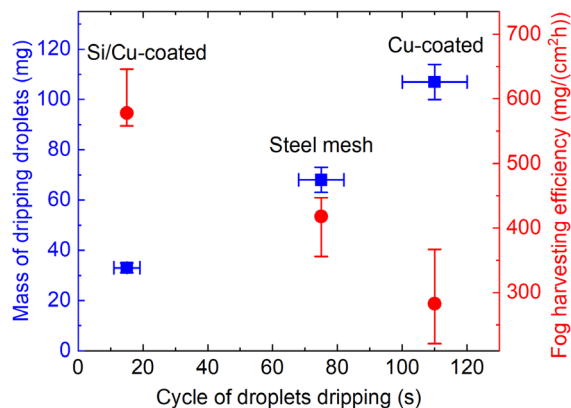
and Cu-coated mesh weighed ≈60–100 mg, the lightest droplets dripped from the Si-/Cu-coated mesh, weighing ≈70% less than those from the other two samples. Due to the low surface energy and superhydrophobicity of the Si-/Cu-coated mesh, these droplets drained more easily, resulting in a drainage time that was three times faster than that of the steel mesh and five times faster than the Cu-coated mesh. In contrast, the largest and slowest-dripping droplets were observed on the Cu-coated mesh.

The right vertical axis in Figure 7 shows the fog water harvesting efficiency of three selected samples—steel, Cu-coated, and Si-/Cu-coated meshes—after five repetitions of test, under the same conditions as described in Section 3.1, with a fixed wind speed of $0.3\,\mathrm{m\,s^{-1}}$. The tests revealed that the Si-/Cu-coated mesh demonstrated significantly higher fog water harvesting efficiency compared to the other two meshes, with an average of $\eta = 580\,\mathrm{mg\,cm^{-2}h^{-1}}$. The fog water harvesting efficiency of Cu-coated mesh exhibits an average of $\eta = 283\,\mathrm{mg\,cm^{-2}h^{-1}}$, while the steel mesh shows an average of $\eta = 418\,\mathrm{mg\,cm^{-2}h^{-1}}$. A 40% increase in fog water harvesting efficiency observed in the Si-/Cu-coated mesh compared to the uncoated mesh is due to its high superhydrophobicity, minimal pore clogging, excellent wetting sustainability, and significantly faster and more efficient fog collection, as demonstrated by data provided in Figure 3–7. Interestingly, the lowest efficiency was observed for the Cu-coated mesh, which exhibited ≈35% lower efficiency than the uncoated steel mesh. The lower efficiency of the Cu-coated mesh is attributed to the water droplet's reaction with the surface, as observed during the wettability and sustained wetting experiments shown in Figure 5 and 6. As the sample shows a very low sustainability in contact with a single droplet, the reaction is significantly intensified during the 2 h fog water harvesting test under a high fog flow rate. The copper layer quickly absorbs water and reacts within the first few minutes of the experiment, resulting a mesh filled with water and consequently, a slow droplet dripping with higher droplet mass, as described by the mass of dripping droplets and the cycle of droplets dripping in Figure 7 and listed in Table S2, Supporting Information. All these events reduced the fog water harvesting efficiency of the Cu-coated mesh significantly.

Figure 8 shows images taken from the front and backside of the samples during the fog water harvesting tests, as well as from the front side of the samples after the 2 h test. According to these images, the droplets accumulated on the steel mesh and Cu-coated mesh appear large or form a liquid layer. In contrast, the Si-/Cu-coated mesh collects droplets with a much smaller diameter compared to the other two samples. Additionally, there is no noticeable presence of water on the backside of the Si-/Cu-coated mesh, due to its stable superhydrophobicity. The mesh pores are also less filled in this sample after the 2 h experiment. This confirms significantly lower clogging of the mesh pores in the Si-/Cu-coated mesh during the fog water harvesting test. A video recorded during the water harvesting test on the Si-/Cu-coated mesh is included as supporting information.

3.4. Discussion

In our previous observation of single millimeter-sized droplet impacts on mesh surfaces, we found that while highly

Figure 7. The mass of dripping droplets and fog water harvesting efficiency of samples versus the cycle of droplets dripping.
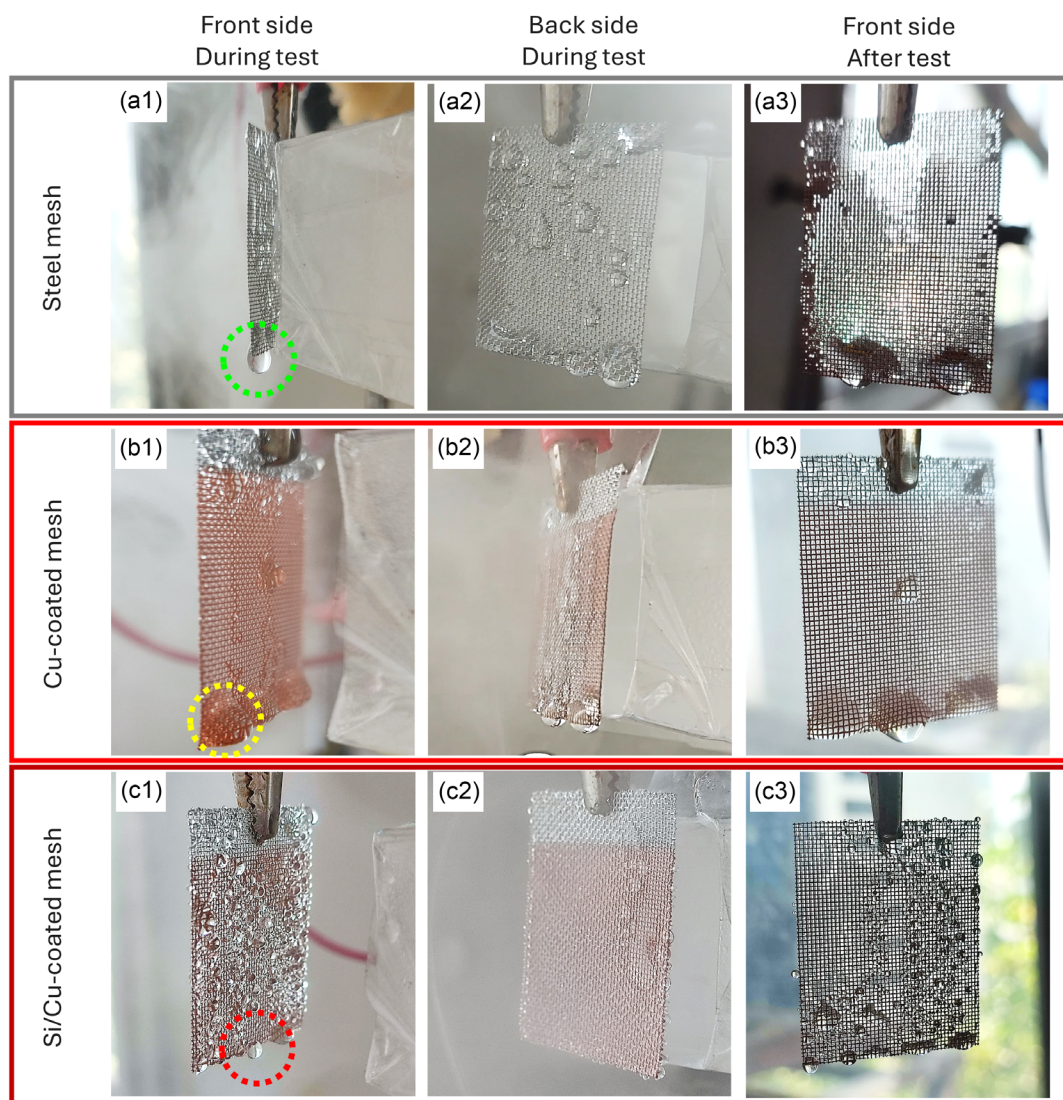
Figure 8. Images taken from water droplets on the samples during the fog collection test: a1–a3), b1–b3), and c1–c3) correspond to steel, Cu-coated, and Si-/Cu-coated meshes, respectively. The images in (a1–c1) were taken from the front side of the mesh at the front of the fog tunnel during the fog collection test. The images in (a2–c2) were taken from the backside of the mesh at the same time as the previous images. The images in (a3–c3) were taken from the front side of the mesh after two hours of the fog collection test. The detaching water droplets from the meshes are indicated by dotted colored circles in (a1–a3).

hydrophobic meshes showed high water collection efficiency, increasing superhydrophobicity led to greater droplet rebound and eventually re-entrainment of water in air.[50] As a result of that study, one could have speculated that achieving higher harvesting efficiency would require a hydrophobic coating. However, the present study indicates that fog water harvesting efficiency generally improves with smaller droplet mass and shorter intervals between droplet drippings. This optimal state occurs when the interaction between the surface and the droplet (adhesion force) is minimal, as seen in superhydrophobic samples like the Si-/Cu-coated mesh. In these cases, droplets detach more easily, facilitating the downward flow of smaller droplets and enhancing fog water harvesting efficiency.[13,20,21,42] In contrast, high surface energy in steel and Cu-coated meshes results

in stronger adhesion, leading to slower droplet drainage and decreased efficiency. This effect is particularly pronounced in Cu-coated meshes, where the copper layer absorbs water and becomes highly hydrophilic, causing droplets to spread and potentially clog the surface. As mesh pores fill, adhesion increases, making drainage more difficult. Additionally, liquid can become trapped in the pores, further hindering drainage. The mesh structure provides a larger surface area for droplet absorption, increasing adhesion forces compared to flat surfaces. As a result, droplets require more mass to overcome surface tension and detach, leading to slower drainage and larger dripping droplets. The highest fog water harvesting efficiency achieved in our research is $580 \, \text{mg} \, \text{cm}^{-2} \text{h}^{-1}$, equivalent to $140 \, \text{L} \, \text{m}^{-2} \text{day}^{-1}$, 14% of the generated fog. This represents a

40% improvement in fog water harvesting efficiency compared to stainless steel mesh.

A detailed comparison between our results and other studies in the field of fog water harvesting, which used similar sample preparation and test design, is provided in **Table 2**, sorted by the publication year. The table includes information on the wettability state of the samples, environmental conditions, fog characteristics, and fog water harvesting efficiencies. According to Table 2, Wang et al. investigated fog water harvesting in superamphiphobic coatings made of SiC particles wrapped in polymers and sprayed onto surfaces.[26] Under fog water harvesting tests with a very high fog flow rate of 216 L h^{-1} and a distance of 18 cm between the sample and the fog outlet, their samples exhibited a fog water harvesting efficiency of 67 L m^{-2}day^{-1}, which is roughly half of the efficiency achieved in the present study. Kang et al. reported a fog water harvesting efficiency of 48 L m^{-2}day^{-1} for superhydrophobic meshes.[34] However, since the fog flow rate and environmental humidity were not provided in their article, it is difficult to confidently compare their results with those of other studies listed here. In another research, Zhou et al. investigated Janus meshes with superhydrophobicity on one side and superhydrophilicity on the other.[51] They observed a maximum fog water harvesting efficiency of 178 L m^{-2}day^{-1}, higher than the present study, though the effect of wind speed was not examined. Sun et al. presented superhydrophobic–hydrophilic patterned surfaces created by punching holes in paper and attaching it to an aluminum sheet, with varying hole sizes and distances.[42] In their study, which tested fog collection efficiency under a relatively low fog flow rate, they reported a maximum fog water harvesting efficiency of 87 L m^{-2}day^{-1}, which is lower than the efficiency achieved in the present study.

In a study by Zhang et al. a complex coating was fabricated by anchoring hydrophilic carbon nanospheres and carbon nanotubes on the surface of PU nanofiber membranes.[52] This study achieved to a very high fog water harvesting efficiency, 400 L m^{-2}day^{-1}, compared to the rest of the reports in this field, with no data on fog flow rate. A similarly high fog water harvesting efficiency was observed by Lee et al. who used 3D-printed poly (lactic acid) (PLA) meshes with different millimeter-sized holes to study the effect of clogging.[53] The prepared hydrophobic meshes were then hydrophilized on one side using oxygen-plasma etching. Their study reported a maximum fog water

harvesting efficiency of 208 L m^{-2}day^{-1}, through the reported plots. However, in both of these later studies,[52,53] the fog flow rate—one of the most important parameters in fog water harvesting experiments—was not reported, making direct comparisons difficult. Lastly, Showket et al. fabricated smooth and rough hydrophilic and hydrophobic steel meshes using vapor deposition and chemical etching.[54] They also investigated the impact of mesh aging under environmental conditions on fog water harvesting efficiency. Their findings showed that rough hydrophilic steel meshes demonstrated the highest fog water harvesting efficiency and sustainability during aging among their samples, with a maximum efficiency of 82 L h^{-1}, which is lower than that achieved in the present study. In their experiments, the fog was provided at the sample location by a wind speed of 0.8 m s^{-1}, which is approximately three times higher than in the present study. As a result of these comprehensive review, the direct comparison between the efficiencies reported in literatures is not straightforward.

Designing effective and scalable fog water harvesters demands a comprehensive approach to address the urgent need for water in arid regions. Developing fog harvester designs that are both practical and cost-effective is crucial for ensuring scalability and accessibility, particularly in resource-limited areas. High performance must be balanced with economic feasibility, considering diverse climates and consistent performance across multiple collection cycles. During research on enhancing fog collection by surfaces, many researchers focus on intricately patterned surfaces fabricated using advanced techniques, achieving high collection efficiency and performance, such as ≈2–3 g cm^{-2}h^{-1} reported by Samanta et al.[55] and Bai et al.[56] under controlled conditions; however, these designs often fall short when translated to real-world applications. Meshes and nets offer a promising alternative for fog harvesting due to their open-porous structure, which allows wind and noncaptured liquid to pass through, and simple structure. This aerodynamic design minimizes clogging, facilitates drainage, enhances wetting recovery, and improves sustainability. The capillary effect in meshes further supports water collection within the pores. Compared to patterned surfaces, which often rely on expensive, high-tech fabrication methods, meshes and nets are low-cost, robust, and supported by well-established industrial fabrication and modification techniques.

Table 2. A comparison between various research studies in the field of fog water harvesting with similar samples and test chamber designs to the present study.

Reference	Wettability	Temperature [°C]	Humidity [%]	Distance [cm]	Fog flow rate [L h^{-1}]	Wind speed [m s^{-1}]	η [mg cm^{-2}h^{-1}]	η [L m^{-2}day^{-1}]
[26]	Superhydrophobic/hydrophilic	22	95	18	216	0.6	280	67
[34]	Superhydrophobic	20	–	1	–	1.7	200	48
[51]	Superhydrophobic/ superhydrophilic	24	95	7	0.16	–	740	178
[42]	Hydrophobic/hydrophilic	20	–	5	0.05	–	362	87
[52]	Hydrophobic/hydrophilic	20	75	5	–	0.5	1666	400
[53]	Hydrophilic/superhydrophilic	20	80	5	–	1.3	865	208
[54]	Hydrophilic	25	92	18	0.14	0.8	341	82
Present study	Superhydrophobic	33	80	15	0.21	0.3	580	140

Yet, many studies on fog water harvesting using meshes, including refs. [48,51,52] mentioned in Table 2, share a common issue: they do not specify the fog flow rate within the test chamber and report extremely high water harvesting efficiencies. As such, fog collection efficiency can be potentially overestimated, as high value may just reflect high fog flow rate, and not the use of efficient surfaces. Indeed, real-world fog collectors, such as those in Chile, produce a maximum of $12 \, L/m^{-2}day^{-1}$ of freshwater.[11] The presence of these disparate reports in the field of fog water harvesting highlights the urgent need to establish standardized testing protocols. These standards should consider the following factors: 1) the amount of water generated by the humidifier, 2) the amount of water that reaches the sample surface, and 3) the amount of water collected by the surface. Moreover, it is necessary to redefine fog water harvesting efficiency by calculating the ratio of the water collected by the surface to the amount of water reaching the surface. To ensure meaningful comparisons, the fog water harvesting performance of improved surfaces should be evaluated against that of untreated surfaces. It is also crucial to systematically investigate the effect of fog flow rate on harvesting efficiency to align experimental results more closely with real-world conditions. Tests should be conducted at lower fog flow rates, with wind speed, temperature, and humidity that mirror actual environments. To achieve this, it is recommended that fog water harvesting test conditions be standardized to more accurately reflect real-world environments: 1) temperature: 5–40 °C, 2) humidity: 50–80%, 3) wind speed: $<5 \, m \, s^{-1}$, 4) fog flow rate: $<0.5 \, L \, h^{-1}$, and 5) droplet size: 3–40 µm.[7,9,11,27,57] Only tests conducted under similar conditions, including droplet size, wind speed, fog flow rate, temperature, and humidity in the vicinity of the sample surface, should be compared. Without such standardization, current results introduce significant noise into this field of study and divert research efforts from the ultimate goal: applying these surfaces for atmospheric water harvesting in real environments to help mitigate water scarcity. In addition, a thorough evaluation of long-term sustainability and resistance to environmental condition is vital for sustained performance. Ultimately, this integrated approach will yield practical, high-performance fog harvesters capable of addressing water scarcity in varied climates, ensuring both immediate impact and long-term sustainability.

For a more realistic perspective on the fog water harvesting efficiency values reported in the literature and their potential application in real-world, it is essential to estimate the amount of atmospheric water available in an area with average fog conditions. Yearly weather forecasts and atmospheric measurement reports suggest that, in a humid environment, a maximum of 8.27 cm of atmospheric water, referred to as 8.27 atm-cm, is available in a vertical column of atmosphere 100 km in length and $1 \, m^2$ in surface area.[7,9,57] If all of this water is collected on the Earth's surface beneath the air column during a day, the maximum fog collection efficiency in a real environment using a surface with optimal morphological and material characteristics would be $82 \, L \, m^{-2}day^{-1}$. However, in many coastal areas like California, where conditions are less favorable, the maximum collection efficiency is reported to be much lower, around $5 \, L \, m^{-2}day^{-1}$.[27] Despite this, improvements in fog water harvesting efficiency from surface modifications measured in a constant test conditions are still noteworthy. For example, the surface morphology and wettability modifications in the present study increased fog water harvesting efficiency by 40%. As a result, this surface could potentially increase the yield to around $\approx18 \, L \, m^{-2}day^{-1}$ in Chile's coast, which equates to less than 20% of the maximum available global atmospheric water.

4. Conclusion

In this study, hydrophobic meshes were fabricated by electrodepositing copper onto meshes, followed by a silica-sol modification to achieve superhydrophobicity. The effects of surface morphology, wettability, and test conditions on the durability and fog water harvesting efficiency of these meshes were evaluated. Results showed that Cu-coated meshes without silica modification had low durability and quickly lost performance under high fog flow. In contrast, silica-coated meshes demonstrated significantly improved sustained wetting and maintained stable superhydrophobicity, even during prolonged tests. The Si-/Cu-coated meshes achieved a 40% higher fog water harvesting efficiency than uncoated meshes. We observed an inverse correlation between fog water harvesting efficiency and three parameters: 1) the time taken for the first droplet to drain from the mesh surface, 2) the mass of the drained droplet, and 3) the time intervals between successive droplet drainages. These parameters are much smaller in Si-/Cu-coated superhydrophobic meshes compared to uncoated and Cu-coated meshes.

We compared various reports on fog water harvesting efficiency, focusing on comparable sample preparations and chamber designs. Our findings highlight a significant overestimation of efficiencies in some reports, primarily due to intensive testing conditions such as unrealistically high fog flow rates. To address this, we introduced a refined calculation method that accounts for both the available atmospheric water and collected water, offering a more accurate representation of performance. Recognizing the need for reliable and scalable solutions, we proposed standardized testing protocols that better reflect real-world fog densities, flow rates, and environmental conditions. This ensures the development of fog water harvesters that are practical and applicable in diverse climates.

Additionally, we emphasize the importance of balancing high performance with economic viability and material availability to support adoption in water-scarce regions, recognizing that laboratory-reported efficiencies may not directly translate to real-world scenarios. By optimizing surface properties and enhancing durability, fog harvesters can deliver improved performance over unmodified surfaces. This integrated approach, encompassing design, testing, and accounting for scalability, paves the way for the development of high-performance fog harvesting systems capable of addressing water scarcity with both immediate and long-term impacts.

Supporting Information

Supporting Information is available from the Wiley Online Library or from the author.

Conflict of Interest

The authors declare no conflict of interest.

Author Contributions

Pegah Sartipizadeh: investigation (lead); methodology (equal); validation (equal); visualization (equal); writing—original draft (equal). **Mohammad Reza Mohammadizadeh**: funding acquisition (equal); project administration (lead); supervision (lead); writing—review & editing (supporting). **Carlo Antonini**: conceptualization (supporting); funding acquisition (equal); writing—review & editing (equal). **Raziyeh Akbari**: conceptualization (lead); data curation (equal); funding acquisition (equal); methodology (lead); visualization (supporting); writing—original draft (equal).

Data Availability Statement

The data that support the findings of this study are available from the corresponding author upon reasonable request.

Keywords

[1] M. Salehi, *Environ. Int.* **2022**, *158*, 106936.
[2] D. Gurera, B. Bhushan, *Philos. Trans. R. Soc., A* **2020**, *378*, 20190444.
[3] J. Olivier, *Water SA* **2002**, *28*, 349.
[4] H. Jarimi, R. Powell, S. Riffat, *Int. J. Low-Carbon Technol.* **2020**, *15*, 253.
[5] K. Chen, Y. Tao, W. Shi, *Sustainability* **2022**, *14*, 6244.
[6] A. W. Kandeal, A. Joseph, M. Elsharkawy, M. R. Elkadeem, M. A. Hamada, A. Khalil, M. Eid Moustapha, S. W. Sharshir, *Sustainable Energy Technol. Assess.* **2022**, *52*, 102000.
[7] P. Yuan, G. Blewitt, C. Kreemer, W. C. Hammond, D. Argus, X. Yin, R. Van Malderen, M. Mayer, W. Jiang, J. Awange, H. Kutterer, *Earth Syst. Sci. Data* **2023**, *15*, 723.
[8] H. Larrain, F. Velásquez, P. Cereceda, R. Espejo, R. Pinto, P. Osses, R. Schemenauer, *Atmos. Res.* **2002**, *64*, 273.
[9] F. Lobos-Roco, F. Suárez, F. Aguirre-Correa, K. Keim, I. Aguirre, C. Vargas, F. Abarca, C. Ramírez, R. Escobar, P. Osses, C. del Río, *J. Arid Environ.* **2024**, *221*, 105125.
[10] B. S. Kennedy, J. B. Boreyko, *Adv. Funct. Mater.* **2023**, *34*, 2306162.
[11] M. Fessehaye, S. A. Abdul-Wahab, M. J. Savage, T. Kohler, T. Gherezghiher, H. Hurni, *Renewable Sustainable Energy Rev.* **2014**, *29*, 52.
[12] Y. Su, L. Chen, Y. Jiao, J. Zhang, C. Li, Y. Zhang, Y. Zhang, *ACS Appl. Mater. Interfaces* **2021**, *13*, 26542.
[13] H. Lu, W. Shi, Y. Guo, W. Guan, C. Lei, G. Yu, *Adv. Mater.* **2022**, *34*, 2110079.
[14] Y. Xiao, J. Huang, Z. Guo, W. Liu, *Mater. Today Phys.* **2022**, *28*, 100869.
[15] F. Lv, F. Zhao, D. Cheng, Z. Dong, H. Jia, X. Xiao, D. Orejon, *Adv. Colloid Interface Sci.* **2022**, *299*, 102564.
[16] D. Nioras, K. Ellinas, V. Constantoudis, E. Gogolides, *ACS Appl. Mater. Interfaces* **2021**, *13*, 48322.
[17] Z. Ahrestani, S. Sadeghzadeh, H. B. Motejadded Emrooz, *RSC Adv.* **2023**, *13*, 10273.
[18] S. Mahat, A. Kumar Jha, K. Darlami, *Proc. IOE Grad. Conf.* **2019**, *6*, 389.
[19] P. Gandhidasan, H. I. Abualhamayel, *Pure Appl. Geophys.* **2012**, *169*, 1019.
[20] Y. Jiang, C. Machado, K. K. Park, *Droplet* **2023**, *2*, e55.
[21] C. Li, B. Kim, J. Yoon, S. Sett, J. Oh, *Adv. Funct. Mater.* **2024**, *34*, 2308265.
[22] W. Shi, M. J. Anderson, J. B. Tulkoff, B. S. Kennedy, J. B. Boreyko, *ACS Appl. Mater. Interfaces* **2018**, *10*, 11979.
[23] J. Park, C. Lee, S. Lee, H. Cho, M. W. Moon, S. J. Kim, *Soft Matter* **2021**, *17*, 136.
[24] R. S. Schemenauer, P. I. Joe, *Atmos. Res.* **1989**, *24*, 53.
[25] D. M. Fernandez, A. Torregrosa, P. S. Weiss-Penzias, B. J. Zhang, D. Sorensen, R. E. Cohen, G. H. McKinley, J. Kleingartner, A. Oliphant, M. Bowman, *Aerosol Air Qual. Res.* **2018**, *18*, 270.
[26] X. Wang, J. Zeng, X. Yu, Y. Zhang, *J. Mater. Chem. A* **2019**, *7*, 5426.
[27] C. Hiatt, D. Fernandez, C. Potter, *Atmos. Clim. Sci.* **2012**, *2*, 525.
[28] A. A. Elshennawy, M. Y. Abdelaal, A. M. Hamed, M. M. Awad, *Water Resour. Manage.* **2023**, *37*, 6107.
[29] A. A. Zefrehei, M. Sheikhzadeh, A. R. Pishevar, *J. Ind. Text.* **2022**, *51*, 3466S.
[30] Y. Wan, Z. Yang, G. Zhang, Y. Wang, *Adv. Eng. Mater.* **2024**, *26*, 2302240.
[31] Y. Wang, L. Zhang, J. Wu, M. N. Hedhili, P. Wang, *J. Mater. Chem. A* **2015**, *3*, 18963.
[32] K. Yin, K. Du, X. Dong, C. Wang, J.-A. Duan, J. He, *Nanoscale* **2017**, *9*, 14620.
[33] K.-C. Park, S. S. Chhatre, S. Srinivasan, R. E. Cohen, G. H. McKinley, *Langmuir* **2013**, *29*, 13269.
[34] J. H. Kang, J.-W. Lee, J. Y. Kim, J. W. Moon, H. S. Jang, S. Y. Jung, *Front. Phys.* **2021**, *9*, 680641.
[35] A. Almasian, G. Chizari Fard, M. Mirjalili, M. Parvinzadeh Gashti, *J. Ind. Eng. Chem.* **2018**, *62*, 146.
[36] V. A. Ganesh, A. S. Ranganath, A. Baji, H. K. Raut, S. Rahay, S. Ramakrishna, *Macromol. Mater. Eng.* **2017**, *302*, 1600387.
[37] B. Yu, H. Hu, J. Li, X. Ding, Z. Li, *Adv. Eng. Mater.* **2024**, *26*, 2400200.
[38] R. Akbari, G. Godeau, M. Mohammadizadeh, F. Guittard, T. Darmanin, *J. Bionic Eng.* **2019**, *16*, 719.
[39] R. Akbari, M. R. Mohammadizadeh, C. Antonini, F. Guittard, T. Darmanin, *Coatings* **2022**, *12*, 1260.
[40] F. Wang, X. Wang, A. Xie, Y. Shen, W. Duan, Y. Zhang, J. Li, *Appl. Phys. A* **2012**, *106*, 229.
[41] R. Feng, F. Song, C. Xu, X.-L. Wang, Y.-Z. Wang, *Chem. Eng. J.* **2021**, *422*, 130119.
[42] R. Sun, J. Zhao, C. Liu, N. Yu, J. Mo, Y. Pan, D. Luo, *Prog. Org. Coat.* **2022**, *171*, 107016.
[43] D. J. Preston, N. Miljkovic, J. Sack, R. Enright, J. Queeney, E. N. Wang, *Appl. Phys. Lett.* **2014**, *105*, 011601.
[44] J. Tam, G. Palumbo, U. Erb, G. Azimi, *Adv. Mater. Interfaces* **2017**, *4*, 1700850.

[45] A. C. Hassebrook, *MS Thesis*, Mechanical and Materials Engineering, University of Nebraska-Lincoln, Nebraska, USA **2017**.

[46] J. Oh, D. Orejon, W. Park, H. Cha, S. Sett, Y. Yokoyama, V. Thoreton, Y. Takata, N. Miljkovic, *iScience* **2022**, *25*, 103691.

[47] A. Diouf, T. Darmanin, S. Y. Dieng, F. Guittard, *J. Colloid Interface Sci.* **2015**, *453*, 42.

[48] C. E. Bauer, R. Speiser, J. P. Hirth, *Metall. Trans. A* **1976**, *7A*, 75.

[49] R. Akbari, G. Godeau, M. Mohammadizadeh, F. Guittard, T. Darmanin, *Appl. Surf. Sci.* **2020**, *503*, 144094.

[50] R. Akbari, Y. Wei, A. Bagni, R. Ruffo, M. J. Thoraval, L. Chen, C. Antonini, *Phys. Fluids* **2024**, *36*, 027137.

[51] W. Zhou, C. Zhou, H. Yang, J. Wang, J. Du, L. Chen, H. Shen, L. Tan, L. Dong, X. Zeng, *J. Environ. Chem. Eng.* **2021**, *9*, 105899.

[52] Y. Zhang, Y. Cai, J. Shi, H. Morikawa, C. Zhu, *Desalination* **2022**, *540*, 115975.

[53] J. H. Lee, Y. J. Lee, H.-Y. Kim, M.-W. Moon, S. J. Kim, *ACS Appl. Mater. Interfaces* **2022**, *14*, 21713.

[54] J. Showket, S. Majumder, N. Kumar, S. Sett, P. S. Mahapatra, *Micro Nano Eng.* **2024**, *22*, 100236.

[55] A. Samanta, W. Huang, H. Ding, *J. Manuf. Processes* **2023**, *98*, 351.

[56] H. Bai, L. Wang, J. Ju, R. Sun, Y. Zheng, L. Jiang, *Adv. Mater.* **2014**, *26*, 5025.

[57] M. Quante, V. Matthias, *J. Phys. IV* **2006**, *139*, 37.